American Mineralogist, Volume 75, pages 667–675, 1990

High-pressure DTA study of the upper three-phase region in the system Na_2CO_3-H_2O

A. F. Koster van Groos
Department of Geological Sciences, University of Illinois at Chicago, Chicago, Illinois 60680, U.S.A.

Abstract

The join Na_2CO_3-H_2O was investigated at 100–925 °C and 0.4–3.7 kbar, using high-pressure differential thermal analysis. The melting reaction of anhydrous Na_2CO_3, which occurs at 851 °C at 1 atm, has a slope of 16.4 ± 0.3 °C/kbar. In the join Na_2CO_3-H_2O the temperature of the vapor-saturated melting reaction involving the upper three-phase assemblage Na_2CO_3 + liquid + vapor decreases with increasing pressure until the reaction terminates at the second critical end point, located at 500 ± 10 °C, 1.505 ± 0.01 kbar and having an H_2O content of 88 ± 2 wt%. These results indicate that Na-rich H_2O-CO_2 supercritical fluids can be present in the upper crust. Because K-rich carbonated supercritical fluids may occur at even lower pressures, the experimental evidence confirms that the intense alkali metasomatism associated with most carbonatite magmas is likely to occur at shallow levels and is dominated by K at very low pressures and by Na at moderately higher pressures. Furthermore, it is concluded that at much higher pressures complex, dense, supercritical alkali-rich H_2O-CO_2 fluids can exist that may contain substantial amounts of alkaline earths. These fluids may have an essential role in the generation and evolution of compositionally highly variable carbonatitic and kimberlitic magma, in addition to being potentially important metasomatic agents in the mantle.

Introduction

Carbon dioxide, water, and alkalis are essential components in carbonatite and kimberlite complexes. Their phase relations, therefore, are important for the understanding of the evolution of these complexes. The system Na_2O-CO_2-H_2O is of special interest, considering the eruption of natro-carbonatite lavas at Oldoinyo Lengai (Dawson, 1962; Dubois et al., 1963). Since the first experimental evidence of carbonate-silicate liquid immiscibility was found in the join $NaAlSi_3O_8$-Na_2CO_3-H_2O (Koster van Groos and Wyllie, 1963), the hypothesis that evolving carbonated alkalic silicate magma can produce an immiscible alkali-rich carbonatite melt has received strong support (e.g., Koster van Groos and Wyllie, 1968, 1973; Freestone and Hamilton, 1980; Le Bas, 1981). After crystallization of Ca, Mg, and Fe carbonates, the remaining alkali-rich fluid is thought to produce the intense alkali metasomatism of country rock (fenitization) that is associated with alkali-poor carbonatite and some kimberlite intrusions (Von Eckermann, 1948). It should be noted, however, that in a recent study immiscible alkali-poor carbonate liquid was found to coexist with an aluminous silicate melt (Kjarsgaard and Hamilton, 1988), which suggests that an alkali-rich environment may not be required.

Competing hypotheses for the formation of carbonatite magma also stress the importance of alkalis. The lowering of the melting temperature of Ca- and Mg-rich carbonate assemblages by alkalis facilitates the generation of primary alkali-rich carbonatite liquids under normal mantle conditions (e.g., Koster van Groos, 1975; Wyllie, 1987; Wallace and Green, 1988). This fluxing effect of alkalis should also assist in the production of late-stage carbonatite magma from differentiating carbonated alkali-rich undersaturated siliceous melts (e.g., Wyllie, 1987). Considering the enrichment in alkalis of many kimberlites (Wass, 1979; Scott, 1979), alkali-rich fluids may have a similar role in the formation of kimberlitic magma (Boettcher et al., 1979; Eggler and Wendlandt, 1979; Wyllie, 1980, 1987).

The phase relations in alkali-CO_2-H_2O systems at elevated pressures are poorly known. This is in part because quenched liquids and vapors are difficult to distinguish from coexisting crystalline phases when using traditional quench methods. High-pressure differential thermal analysis (HP-DTA) of such systems (i.e., in systems in which reactions are rapid and easily reversible) is especially effective, as will be shown in this study of the upper three-phase region of the join Na_2CO_3-H_2O.

Previous work

The phase relations in the system Na_2CO_3-NaOH-H_2O to 500 bars and 500 °C (Tranquard, 1965) show that the bounding system NaOH-H_2O exhibits continuous solubility between NaOH and H_2O. However, in the join Na_2CO_3-H_2O the solubility of Na_2CO_3 in the vapor is strongly retrograde, with the critical H_2O-rich fluid containing less than 0.3% Na_2CO_3 (Waldeck et al., 1932).

0003–004X/90/0506–0667$02.00

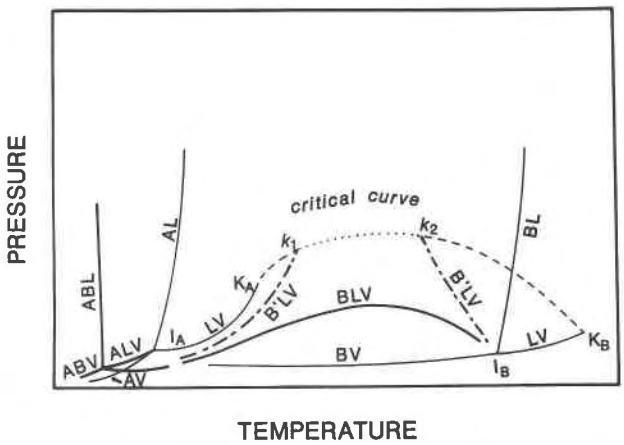

Fig. 1. Schematic *P-T* projection of a binary system A-B, showing the relation between the vapor-saturated solubility curve and the critical curve. For a description, see text.

This indicates that in the join Na_2CO_3-H_2O the vapor-saturated melting curve is intersected by the critical curve, generating two critical end points. The difference between these types of systems is illustrated schematically in Figure 1. Two one-component systems, A and B, each have a triple point, I_A and I_B; a critical point, K_A and K_B; a sublimation reaction, AV and BV; a melting reaction, AL and BL; and a boiling reaction, LV. The binary system A-B has a binary sublimation reaction, ABV, and a melting reaction, ABL. The two critical points K_A and K_B are connected with a critical curve for intermediate compositions. In the first type of system, the vapor-saturated melting of A and B is indicated by the curves ALV and BLV, respectively (solid line). Note that BLV does not intersect the critical curve. This behavior is typical for systems such as NaOH-H_2O. In the second type of system, the curve labeled B'LV (dashed line), which represents the vapor-saturated melting of B, is displaced to higher pressures. The difference here is that B'LV intersects the critical curve, generating two critical end points, k_1 and k_2. This intersection renders the portion of the critical curve between k_1 and k_2 metastable and causes the two segments of the B'LV curve to terminate without metastable extensions. This type of system is typical for many silicate-H_2O systems as well as for a large number of salt-H_2O systems. In the join Na_2CO_3-H_2O, the first critical end point is located very close to the critical point of H_2O. The second critical end point was estimated to lie at pressures above 1000 bars (Morey and Chen, 1956). The latter was supported in a study of the join $NaAlSi_3O_8$-Na_2CO_3-H_2O, where a H_2O-rich vapor phase was found to coexist with a carbonate-rich liquid at 1 kbar pressure (Koster van Groos and Wyllie, 1968). For a review of these critical phenomena, see Ricci (1951) for binary systems and Boettcher and Wyllie (1969) for ternary and quaternary systems.

Experimental work

Apparatus

The apparatus for HP-DTA used in this study has been described in detail by Koster van Groos (1979). In summary, a DTA cell-thermocouple assemblage was made to fit in an internally heated pressure vessel similar to the one described by Holloway (1971). The DTA cell consists of a copper block with positions for three capsules, two for samples and one for a reference; Al_2O_3 powder was used. The capsules, made from gold foil by extrusion, are 10 mm long, have a diameter of 3.2 mm and a wall thickness of 0.07 mm, and weigh approximately 120 mg. A reentry well of about 1 mm depth accommodates a Pt-$Pt_{90}Rh_{10}$ thermocouple that is spring-loaded to ensure thermal contact.

The temperature of the sample is obtained from the reference and corrected using the differential temperature. The corrected temperatures are believed accurate to within 1 °C. In this study the DTA signals were recorded using the 200 μV range of a strip-chart recorder, allowing resolution of temperature deviations to 0.2 °C. Pressures are measured to within 0.5%, using medium- and high-pressure Bourdon-type calibrated Heise gauges. The optimum heating rate was 20 °C/min. Slower heating rates (5–10 °C/min) did not measurably change the observed reaction temperatures, but the peak-height was reduced significantly. The system is regularly calibrated at different pressures using the low quartz–high quartz inversion (Yoder, 1950; Koster van Groos and ter Heege, 1973).

Experimental method

The starting materials used in this investigation were Na_2CO_3 (supplier: Aldrich; purity: 99.999%), dried at 150 °C to constant weight, and distilled water. Both pure Na_2CO_3 and mixtures of Na_2CO_3 and water were used. The sample weight was between 13 and 26 mg. Where compositions contained less than 80 wt% H_2O, the water was inserted into the capsule using a pipette before Na_2CO_3 was added. In the starting compositions with 80, 85, and 92 wt% water, a solution of Na_2CO_3 was used. In the experiments with a high H_2O content, the total weight of the sample was reduced to diminish the chance that the capsules would burst. Nevertheless, capsules usually failed below 0.5 kbar and, consequently, no data are available below this pressure. Most experiments were taken through a series of heating and cooling cycles, beginning at the highest pressures. Pressure was reduced in steps after completion of several cycles until the DTA curve showed anomalous results, such as peak temperatures that are similar to those in the anhydrous experiments, indicating capsule failure.

The information obtained by DTA relates to the rate and amount of heat the sample exchanges with its environment. A reaction in a sample causes a change in this heat balance, which produces a change in the differential temperature. If the change in rate is sufficiently rapid, a peak in the DTA curve results. With a constant reaction

rate, the amount of heat exchanged remains approximately constant, and the temperature differential is constant also. The DTA peak shows the beginning of a reaction (onset), a limb that can be extrapolated to intersect the baseline and that represents the change in the rate of the reaction to a maximum value (extrapolated onset), a peak where the reaction rate is at a maximum, and a limb returning to the baseline when the reaction is terminated. The onset temperature, the extrapolated onset temperature, and the peak temperature all have been used as the temperature of reaction (Smykatz-Kloss, 1974; Wendlandt, 1974; Brown, 1988). In heating curves, the peak temperature (maximum reaction rate) represents the maximum value for the reaction temperature, whereas the extrapolated onset temperature is generally considered as a minimum. In many substances the onset temperature occurs at a significantly lower temperature. Therefore, it is often not representative of the reaction temperature. In this study the cooling curves were used only for establishing a minimum value for a reaction. Because of nucleation problems in melts, onset temperatures in cooling curves in these types of systems are usually significantly below the reaction temperature; cf. Koster van Groos (1979).

In a one-component system in which reaction rates are high, a reaction usually generates a sharp peak. In a multicomponent system, the number of reactants is often more than one, and isothermal invariant reactions tend to proceed at a slower rate because experimental and kinetic parameters such as the grain size of the solid phases, material transport, etc. affect the reaction rate. As a consequence, the peak related to such a reaction is broader, and the determination of a reaction temperature inherently less precise than in a one-component system.

Results

The join Na_2CO_3-H_2O was investigated using samples containing 0, 5, 10, 25, 30, 35, 40, 45, 50, 60, 70, 80, 86, and 92 wt% H_2O. The results are listed in Table 1. In experiments with pure Na_2CO_3 the peaks were extremely sharp, with the temperature of the extrapolated onset only approximately 2 °C lower than the corrected peak temperature. The onset temperature is much less reproducible and was observed 3–12 °C below the extrapolated onset temperature. The melting reaction of pure Na_2CO_3 is linear over the pressure range of the investigation, from 0.5 kbar to 3.7 kbar, and has a slope of 16.4 ± 0.3 °C/kbar (Fig. 5). The 1 atm intersect of the extrapolated onset temperature is at 852.5 ± 1 °C, which is in excellent agreement with the melting temperature of Na_2CO_3 as given by the supplier (Tm = 851 °C). This suggests that the extrapolated onset represents the melting temperature. Extrapolation of the melting temperature to 10 kbar yields a temperature of 1017 ± 4 °C, in good agreement with an earlier determination of 1024 ± 10 °C (Koster van Groos, 1979). Melting of Na_2CO_3, therefore, appears linear over an extensive pressure range. The cooling curves showed a consistent undercooling of 4–5 °C, after which a very sharp peak was produced.

DTA curves of experiments with 5, 10, and 25 wt% H_2O are shown in Figures 2–4, respectively. The peak at 110–125 °C is caused by the dehydration reaction of $Na_2CO_3 \cdot H_2O$ (Waldeck et al., 1932). Occasionally this peak is a doublet, suggesting that dehydration may involve two steps. The next peak represents the beginning of melting; its onset temperature and extrapolated onset temperature almost coincide. Therefore, the onset temperature is taken as the solidus in this join. With a further temperature increase the signal does not return to the baseline but shows a broad reaction, which is interpreted as the dissolution of Na_2CO_3 into the liquid, with the temperature differential proportional to the dissolution rate. The temperature at which the signal returns to the baseline is taken as the liquidus temperature for this composition (Wendlandt, 1974; Eggler and Rosenhauer, 1978; Koster van Groos, 1979). In several DTA curves precise determination of this temperature was not possible, because the DTA signal curved smoothly toward the baseline, and the return temperature was not well defined.

Cooling curves are not shown. They usually show two peaks representing both the liquidus and solidus. The peaks are characteristic of undercooling, with the onset and peak occurring at virtually the same time. Consequently, the corrected peak temperature is higher than the onset temperature, which means that the enthalpy of crystallization heated the sample noticeably. The peak temperatures are 10–25 °C below the liquidus and solidus as determined in the heating experiments. The lack of reproducibility in the cooling peak temperatures is attributed to nucleation problems, which is normal in these types of systems. No peak was observed for the hydration reaction of Na_2CO_3; evidently this reaction is relatively slow.

The DTA curves illustrate the effect of increasing pressure on the solidus and liquidus temperatures. In the series with 5 wt% H_2O (Fig. 2) a pronounced peak at 0.58 kbar represents both the solidus and the dissolution reaction of Na_2CO_3. With increasing pressure this peak broadens and splits into two. The temperature of the first peak, which represents the solidus, decreased substantially, whereas the temperature of the second peak, representing a high rate of dissolution of Na_2CO_3 into the melt, increased. The solidus peak becomes smaller at higher pressures, probably because at higher pressures the H_2O content of the first liquid formed increases, resulting in less melting. At pressures above 1.5 kbar no melting reaction was observed. At each pressure the liquidus temperature of this composition is relatively high and approaches the melting temperature of dry Na_2CO_3.

In the series with 10 and 25 wt% H_2O (Figs. 3 and 4) a similar pattern can be seen. In these runs the melting reaction is much more pronounced. Again, at pressures above 1.5 kbar the melting peak is absent. The liquidus data show that in the experiments with 10 wt% H_2O the liquidus temperature is nearly constant with respect to

TABLE 1. Pressure and temperature of the onset, peaks, and termination of DTA signals in the join Na_2CO_3-H_2O

Experiment	Onset		1st Peak		2nd Peak		Termination	
	P	*T*	*P*	*T*	*P*	*T*	*P*	*T*
Composition: Na_2CO_3								
Series A5: Na_2CO_3: 26.10 mg								
A5-16	500	858	502	864	na	na	504	874
A5-18	805	862	806	868	na	na	nd	nd
A5-4	970	860	976	871	na	na	nd	nd
A5-11	1020	862	1023	871	na	na	1025	880
A5-10	1035	862	1038	872	na	na	1040	882
A5-15	1072	866	1076	872	na	na	1080	882
A5-5	1252	865	1260	875	na	na	nd	nd
A5-14	1505	871	1513	878	na	na	1520	887
A5-13	1875	880	1877	884	na	na	1885	893
A5-1	2005	880	2007	888	na	na	2010	894
A5-6	2262	880	2266	890	na	na	2270	900
A5-12	2975	902	2977	904	na	na	2980	916
A5-9	3740	906	3753	917	na	na	3760	924
Composition: Na_2CO_3 + 5 wt% H_2O								
Series A5: Na_2CO_3: 20.80 mg; H_2O: 1.06 mg; series A7: Na_2CO_3: 19.00 mg; H_2O: 1.00 mg								
A5-16	475	760	no	no	500	850	502	860
A5-17	563	720	569	763	584	833	585	845
A7-3	694	690	708	725	729	795	743	820
A5-3	701	683	743	723	786	795	790	806
A7-2	864	667	866	673	911	795	921	825
A5-4	900	650	907	685	938	777	955	820
A5-11	932	650	938	670	983	795	995	810
A5-10	940	648	949	667	1000	795	1011	805
A5-15	1004	633	1011	660	1050	792	1052	805
A7-7	1100	617	1117	637	1193	790	1203	828
A5-5	1134	610	1145	630	1217	787	1230	800
A5-7	1207	608	no	no	1303	750	1310	805
A5-8	1247	580	1260	602	1361	782	1372	805
A7-6	1320	574	no	no	no	no	no	no
A5-14	1327	562	1340	580	1464	780	1485	814
A7-1	1354	560	1360	575	1510	806	1525	825
A5-2	1437	540	1450	560	1616	790	1636	815
A7-4	1458	540	no	no	1643	803	1650	827
A5-13	no	no	no	no	1805	794	1820	812
A5-6	no	no	no	no	2220	804	2234	814
A5-12	no	no	no	no	2880	805	2888	827
A5-9	no	no	no	no	3637	811	3691	849
Composition: Na_2CO_3 + 10 wt% H_2O								
Series A6: Na_2CO_3: 18.04 mg; H_2O: 2.06 mg								
A6-1	462	74	468	780	481	841	481	848
A6-2	539	720	546	759	553	796	560	810
A6-3	580	716	584	737	587	757	591	780
A6-4	667	689	674	722	679	741	684	765
A6-11	808	667	818	696	835	745	839	752
A6-5	928	650	942	672	960	760	995	790
A6-6	1148	600	1162	625	1231	740	1237	765
A6-7	1362	525	1382	550	no	no	1450	647
A6-8	1396	550	1400	565	1502	725	1520	750
A6-12	1500	no	no	no	no	no	2300	no
A6-10	2300	on	no	no	no	no	3000	no
Composition: Na_2CO_3 + 25 wt% H_2O								
Series A6: Na_2CO_3: 18.04 mg; H_2O: 5.96 mg; series A7: Na_2CO_3: 20.40 mg; H_2O: 6.90 mg								
A6-1	471	793	481	833	no	no	481	842
A6-2	550	767	557	821	no	no	560	828
A6-3	584	735	591	781	595	791	598	800
A6-4	667	685	674	722	680	749	684	766
A7-3	694	695	708	715	no	no	708	729
A6-11	808	667	814	688	827	726	831	735
A7-2	862	663	868	680	no	no	859	715
A6-5	928	645	938	664	950	690	962	720
A7-7	1100	617	1110	630	1135	667	1145	685
A6-6	1148	600	1158	618	1183	660	1190	670
A7-6	1320	570	1326	580	no	no	1403	650
A7-1	1355	569	1375	585	no	no	1420	660
A6-7	1360	520	1382	550	no	no	1395	570
A6-8	1383	540	1402	560	1423	600	1447	640
A7-4	1458	547	1465	555	no	no	no	no
A7-5	1581	no	no	no	no	no	no	no
A6-10	2300	no	no	no	no	no	3000	no

TABLE 1—*Continued*

Experiment	Onset		1st Peak		2nd Peak		Termination	
	P	*T*	*P*	*T*	*P*	*T*	*P*	*T*
Composition: Na_2CO_3 + 30 wt% H_2O								
Series A8: Na_2CO_3: 12.55 mg; H_2O: 5.16 mg								
A8-1	1069	613	1076	638	no	no	1080	673
A8-2	1272	565	1286	585	no	no	1310	623
A8-3	1464	525	1468	535	no	no	1485	610
A8-4	1485	514	1490	520	no	no	1500	530
A8-6	1520	500	1521	503	no	no	1590	no
A8-7	1588	no	no	no	no	no	1680	no
Composition: Na_2CO_3 + 35 wt% H_2O								
Series A8: Na_2CO_3: 12.83 mg; H_2O: 6.91 mg								
A8-1	1069	612	1076	639	no	no	1080	666
A8-2	1272	565	1286	585	no	no	1310	623
A8-3	1464	525	1468	535	no	no	1478	590
A8-4	1485	514	1490	520	no	no	1500	530
A8-6	1500	no	1520	505	no	no	1590	no
A8-7	1588	no	no	no	no	no	1680	no
Composition: Na_2CO_3 + 40 wt% H_2O								
Series A9: Na_2CO_3: 7.82 mg; H_2O: 5.25 mg								
A9-3	1330	555	1341	575	no	no	1354	600
A9-2	1398	534	1409	550	no	no	1430	580
A9-7	1427	532	1433	540	no	no	1478	593
A9-1	1433	526	1440	540	no	no	1480	590
A9-4	1490	520	1492	522	no	no	no	no
Composition: Na_2CO_3 + 45 wt% H_2O								
Series A9: Na_2CO_3: 8.31 mg; H_2O: 6.59 mg								
A9-3	1330	555	1341	575	no	no	1350	585
A9-2	1398	534	1409	550	no	no	1423	570
A9-7	1427	532	1433	540	no	no	1443	560
A9-1	1433	530	1440	540	no	no	no	no
A9-4	1490	515	1492	520	no	no	no	no
Composition: Na_2CO_3 + 50 wt% H_2O								
Series A10: Na_2CO_3: 7.48 mg; H_2O: 7.32 mg								
A10-1	1289	556	1303	570	no	no	1306	580
A10-5	1540	no	no	no	no	no	no	no
Composition: Na_2CO_3 + 60 wt% H_2O								
Series A10: Na_2CO_3: 7.24 mg; H_2O: 10.76 mg								
A10-1	1289	556	1303	570	no	no	1310	580
A10-4	1420	530	1426	540	no	no	1433	552
A10-3	1499	520	1503	527	no	no	1506	535
A10-5	1540	no	no	no	no	no	no	no
Composition: Na_2CO_3 + 70 wt% H_2O								
Series A11: Na_2CO_3: 7.17 mg; H_2O: 16.33 mg								
A11-7	1313	557	1318	564	no	no	1320	570
A11-5	1526	no	no	no	no	no	no	no
Composition: Na_2CO_3 + 80 wt% H_2O								
Series A11: Na_2CO_3: 3.85 mg; H_2O: 11.49 mg								
A11-7	1313	557	1318	564	no	no	1320	570
A11-6	1410	537	1415	544	no	no	1425	557
A11-1	1444	527	1449	532	no	no	1450	535
A11-3	1471	518	1475	525	no	no	1480	530
A11-2	1492	508	1495	510	no	no	1500	515
A11-4	1509	503	1510	505	no	no	1515	510
A11-5	1526	no	no	no	no	no	no	no
Composition: Na_2CO_3 + 86 wt% H_2O								
Series A12: Na_2CO_3: 1.91 mg; H_2O: 11.71 mg								
A12-1	1282	560	1289	568	no	no	1290	570
A12-2	1348	548	1355	555	no	no	1360	560
A12-4	1502	490	1505	495	no	no	1585	590
A12-3	1502	490	1505	495	1580	590	1595	610
Composition: Na_2CO_3 + 92 wt% H_2O								
Series A12: Na_2CO_3: 1.067 mg; H_2O: 12.27 mg								
A12-2	1344	541	1345	543	no	no	1360	560
A12-4	1495	490	1498	495	no	no	1500	500

pressure whereas with 25 wt% H_2O it decreases significantly.

These DTA curves also show the dehydration reaction of $Na_2CO_3 \cdot H_2O$. It was encountered at 115 °C and 0.34 kbar and at 134 °C and 2.100 kbar (second peak temperature for double peaks). Determinations at intermediate

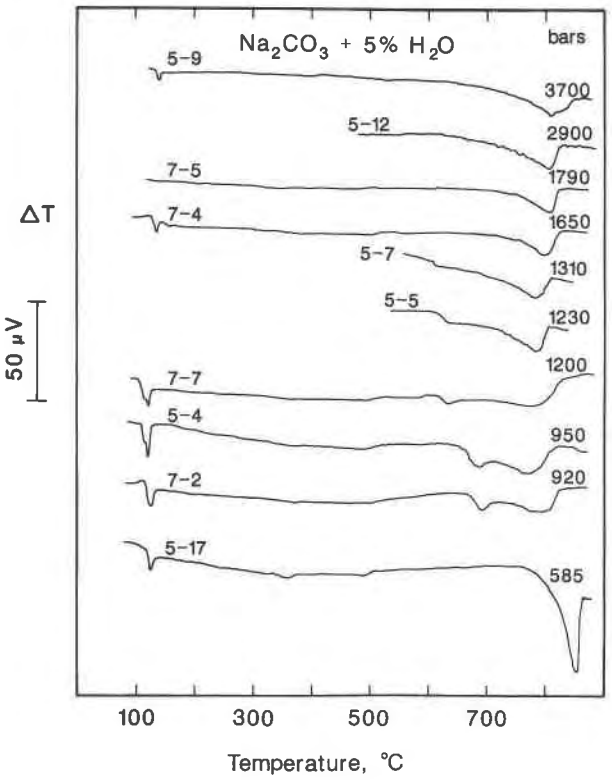

Fig. 2. HP-DTA curves for runs with 95 wt% Na_2CO_3 and 5 wt% H_2O at pressures to 3.7 kbar. A signal of 50 μV represents a differential temperature of approximately 5 °C. On the right the final pressure is shown. The experiments are listed in Table 1.

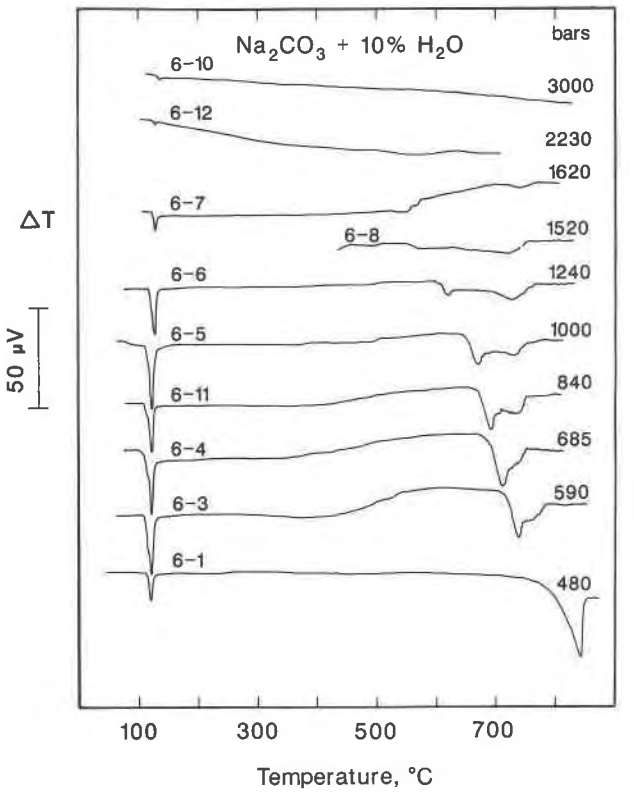

Fig. 3. High-pressure DTA curves for experiments with 90 wt% Na_2CO_3 and 10 wt% H_2O at pressures to 3 kbar. A signal of 50 μV represents a differential temperature of approximately 5 °C. On the right the final pressure is shown. The experiments are listed in Table 1.

pressures show that its slope is linear (10.8 ± 1 °C/kbar). Extrapolation of this reaction results in a dehydration temperature of 111.5 ± 1 °C at 1 atm, which is in excellent agreement with an earlier determination of 112.5 ± 1 °C (Waldeck et al., 1932).

The solidus temperature at a given pressure, defined as the onset temperature, is not affected noticeably by even a large increase in the sample's water content (Table 1). However, in experiments with 86 wt% H_2O, the onset temperature is reduced slightly, and with 92 wt% H_2O present it is even lower. The temperatures at which the liquidus reaction terminates decrease rapidly with higher H_2O contents, and eventually the onset, peak, and return temperatures almost coincide. However, in several experiments with 86 wt% H_2O the return temperature increased substantially, suggesting that the field (L + V) was intersected.

The data compiled in Table 1 are presented in Figure 5. The temperature and pressure of the solidus define the vapor-saturated melting curve. Shown also are the liquidus curves for compositions containing between 5 and 45 wt% H_2O and the melting curve of pure Na_2CO_3. The most important result is the disappearance of the solidus reaction with increasing pressure. The only reasonable explanation is that the melting reaction (NC + V = L) is no longer present. This means that the liquid and vapor phases become identical and that the three-phase curve terminates at a second critical end point. The location of this point was determined using a series of experiments near 1.5 kbar; it lies at 500 ± 10 °C and 1.505 ± 0.01 kbar. The critical fluid at these conditions is estimated to contain 88 ± 2 wt% H_2O, based on the experiments with 86 wt% H_2O (which have a melting temperature in reasonable agreement with experiments containing less H_2O), and on the experiment with 92 wt% H_2O (A12-4, Table 1) (which has a very weak peak at 490 °C and 1.495 kbar, significantly below the solidus temperature at this pressure). The latter peak probably represents the intersection with the vaporous.

The liquidus curves for the different compositions converge to approximately 850 °C and 0.5 kbar. In a binary system the liquidus curves do not converge but intersect the vapor-saturated melting curve at their saturation pressure. The convergence of the liquidus curves, therefore, indicates that the phase relations in the join are ternary. This is illustrated in Figure 6 with a series of isobaric T-X sections based on the phase relations presented in Figure 5. The liquidus is drawn through the

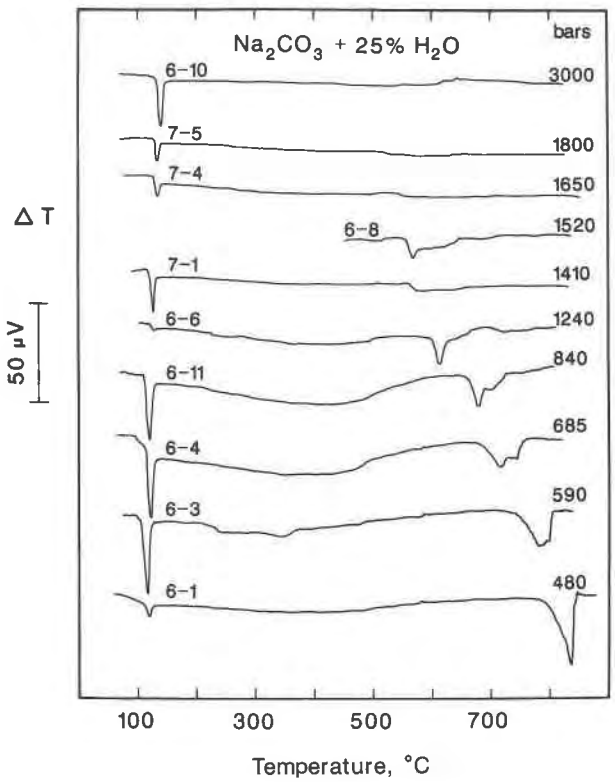

Fig. 4. High-pressure DTA curves for experiments with 75 wt% Na_2CO_3 and 25 wt% H_2O at pressures to 3 kbar. A signal of 50 μV represents a differential temperature of approximately 5 °C. On the right the final pressure is shown. The experiments are listed in Table 1.

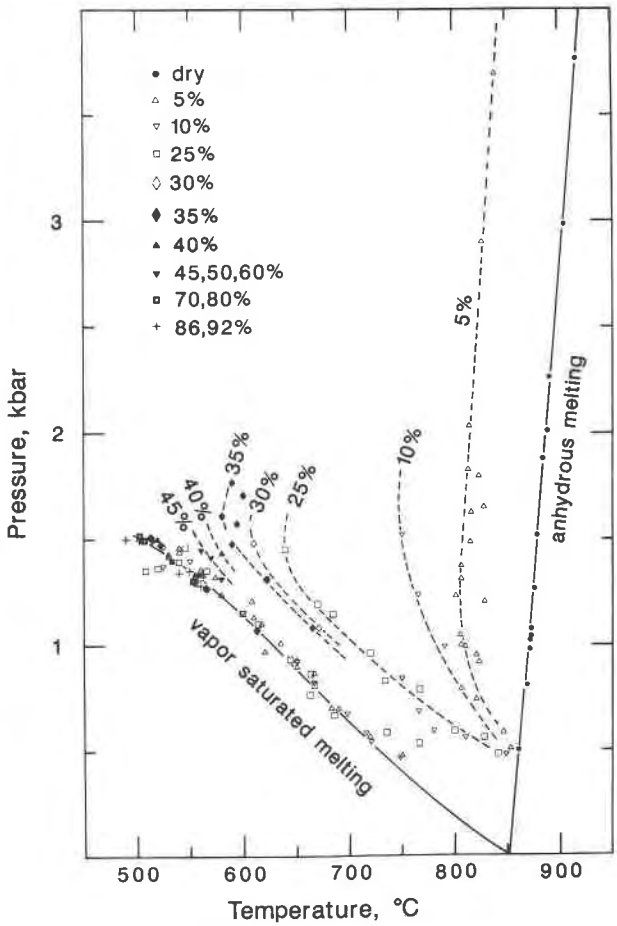

Fig. 5. The upper three-phase region of the join Na_2CO_3-H_2O. Solid lines represent the anhydrous- and vapor-saturated melting of Na_2CO_3. The dashed lines show the liquidus for compositions with 5, 25, 30, 35, 40, and 45 wt% H_2O. The symbols indicate the H_2O-content in wt%.

symbols representing the liquidus temperatures as determined in Figure 5. The section at 0.5 kbar shows that the liquidus, which is the boundary between the phase fields (NC + L) and (L) and between (NC + L + V) and (L + V), is intersected at similar temperatures for compositions containing 5, 10, 25, and 30 wt% H_2O. At higher pressures the difference between the liquidus temperatures for the different compositions increases substantially. Consequently, the liquidus temperatures converge at the lower pressure. In the two-phase fields containing NC, the composition of the coexisting liquid or vapor must lie within the composition join. However, in the three-phase field (NC + L + V) Na_2CO_3 does not dissolve stoichiometrically in the coexisting liquid and vapor phases. Assuming eutectic-type relations in the ternary system, the liquid will be enriched in Na_2O and the vapor phase in CO_2. Because the composition of the solid phase NC is probably almost pure Na_2CO_3, the upper and lower temperature boundaries of the three-phase field, the latter being the solidus, are nearly isothermal. The three-phase field becomes progressively smaller with increasing pressure and terminates at the second critical end point.

Discussion

The temperature, pressure, and composition of the second critical end point in the joint Na_2CO_3-H_2O represents one point on a curve, which is the locus of the second critical end points for different composition joins in the ternary system Na_2O-CO_2-H_2O. Because in the bounding system NaOH-H_2O the vapor-saturated melting curve is continuous (Fig. 1), the second critical end point curve will move to lower pressures for compositions richer in Na_2O-H_2O, whereas in joins richer in CO_2 the pressure of the second critical end point curve should increase rapidly. The first critical end point curve is close to the bounding system H_2O-CO_2, as the solubility of Na_2CO_3 in these vapors is undoubtedly very low. In *P-T* space these two critical end-point curves must meet at a ternary invariant critical point where the three-phase solubility curve becomes continuous. The location of this point is near the system NaOH and H_2O, but its precise temperature, pressure, and composition are not known.

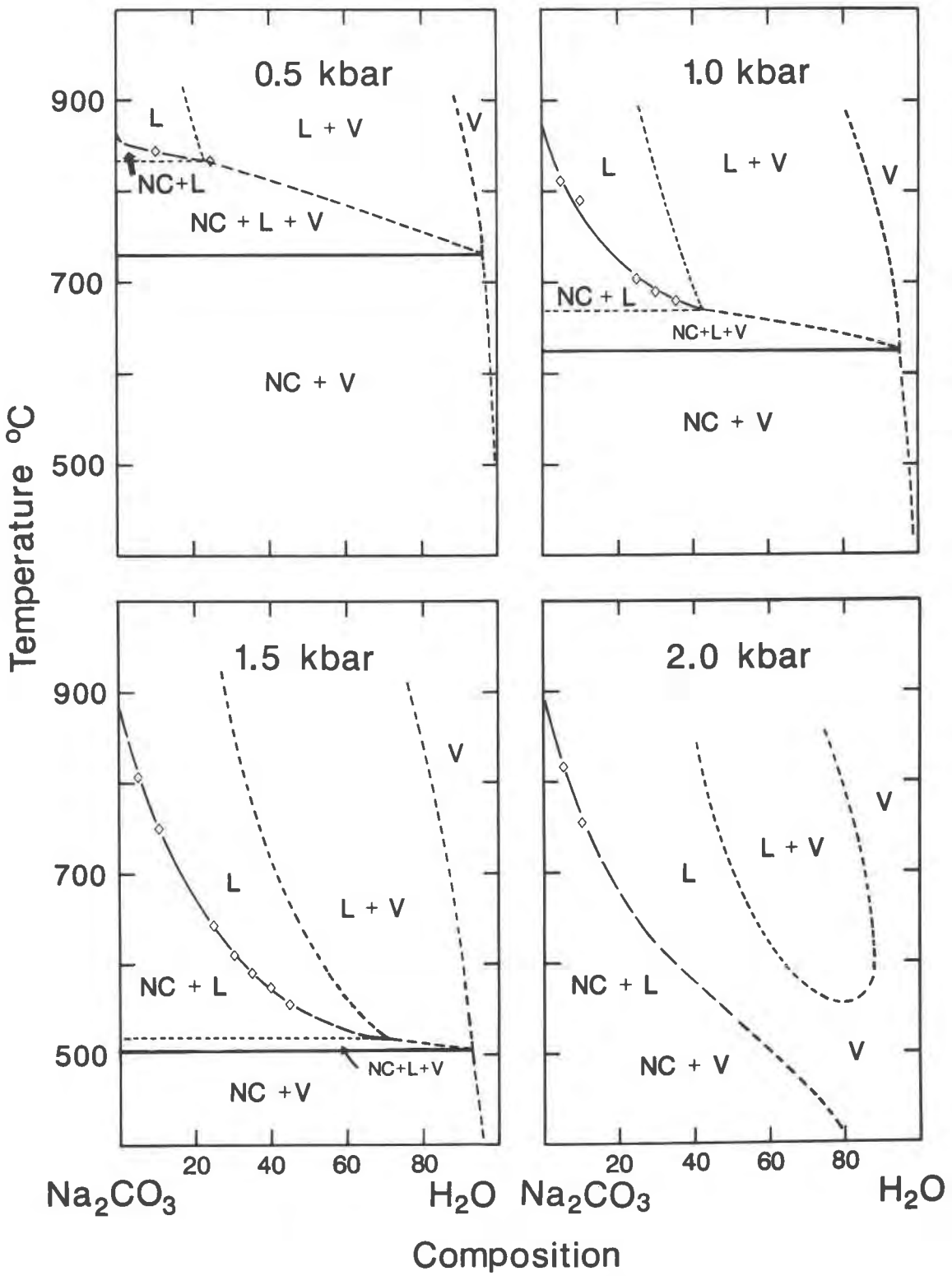

Fig. 6. T-X sections through the join Na_2CO_3-H_2O at 0.5, 1, 1.5, and 2 kbar pressure, based on Fig. 5. The solidus temperature is obtained from the intersection of the isobaric section with the vapor-saturated melting curve. The open symbols, which represent the intersection with the liquidus curves, determine the position of the vapor-undersaturated liquidus. Abbreviations: NC = Na_2CO_3; L = liquid; V = vapor.

In more complex carbonate systems the additional components must significantly affect the pressure and temperature at which Na_2CO_3-rich supercritical fluids are present. For example, the join K_2CO_3-H_2O exhibits continuous solubility (Morey and Chen, 1956). Addition of K_2CO_3 to the join Na_2CO_3-H_2O therefore can be expected to lower the pressure at which supercritical conditions are encountered. In contrast, adding $CaCO_3$ should substantially increase the pressure of the second critical end point, considering that the pressure of the second critical end point in the join $CaCO_3$-H_2O exceeds 40 kbar (Wyllie and Boettcher, 1969). A similar effect can be expected with $MgCO_3$ or $FeCO_3$ (Ellis and Wyllie, 1979). Consequently, the compositions of the fluid phase and the coexisting carbonate assemblage are strongly dependent on pressure. At temperatures of approximately 500–700°C and at a low but increasing pressure, the fluid will be enriched first with K_2CO_3 and later with Na_2CO_3. At much higher *P-T* conditions such fluids may be able to dissolve substantial amounts of $CaCO_3$, $MgCO_3$, and $FeCO_3$.

This study is probably the first in which a second critical end point in a salt-water system was determined using DTA. The precision of the method appears to be good. In contrast, equilibrium experiments in these types of systems do not provide sufficient information to distinguish a liquid-solid assemblage from a dense supercritical fluid-solid assemblage in the absence of characteristic quench products, such as glass, or glassy, perhaps spherical material typical of a quenched volatile-rich fluid. As a consequence, supercritical fluids may remain undetected in equilibrium studies.

Geological applications

There is a wealth of evidence indicating that most carbonatite magmas initially are enriched in alkalis. For example, fluid inclusions in apatite crystallized from carbonatite-melt systems are often rich in K-Na-Ca carbonates (Rankin, 1977), unequivocally establishing that alkali-rich fluids commonly coexist with carbonatite melts. The often extensive fenitization associated with most carbonatite complexes shows that a crystallizing carbonatite magma may produce large amounts of alkali-rich aqueous fluids that are dominated by K at relatively shallow levels (Von Eckermann, 1948) and by Na at deeper levels (Le Bas, 1981). The occurrence of Na_2CO_3-rich lava at Oldoinyo Lengai (Dawson, 1962; Dubois et al., 1963) clearly established that under unusual conditions relatively dry alkali-rich carbonatite may form.

The experimental evidence presented in this study indicates that the composition of alkali-rich CO_2-H_2O fluids can be K- and Na-rich at pressures >1.5 kbar, but that at lower pressures these fluids become K-rich but Na-poor. Consequently, the solubility of Na in an ascending alkali-rich carbonated supercritical fluid decreases rapidly over a small pressure interval. The increase in Na activity could result in the crystallization of Na-rich minerals in wallrock, in a substantial Na-enrichment of a coexisting melt, or perhaps in the formation of a Na_2CO_3-rich magma, e.g., as at Oldoinyo Lengai. Furthermore, the loss of Na from such a fluid would cause it to become relatively K-enriched, which may explain the observed trend from Na- to K-dominated metasomatism in fenitizing fluids associated with carbonatites with decreasing pressure.

The generation of alkaline basalts, kimberlites, and carbonatites that occurs at relatively high pressures probably involves reactions between alkali-rich CO_2-H_2O fluids and the peridotite mantle (Menzies and Wass, 1983; Bailey, 1984; Wendlandt, 1984; Roden and Murthy, 1985; Spera, 1987; Wyllie, 1987). In most models the nature of these fluid phases is rarely specified, and as a result their chemical role is "essentially unconstrained" (Eggler, 1987). Nevertheless, it may be assumed that these fluids preferentially dissolve REE (Wendlandt and Harrison, 1979). It is shown also that the SiO_2 solubility decreases substantially with increasing CO_2 content (Shettel, 1973; Novgorodov, 1975; Walther and Orville, 1983). Furthermore, in CO_2-rich vapors the ratio Na/Al is greater than unity (Schneider and Eggler, 1984, 1986). The effect of other components, such as Cl, F, or P_2O_5, on the solubility is not known for these conditions, but the halogens probably enhance REE partitioning into the fluid because of increasing halogen complexing (Flynn and Burnham, 1978).

As was seen above, at much higher pressures carbonated alkali-rich fluids are probably capable of dissolving substantial amounts of alkaline earths. If the solubility of the alkaline earth carbonates at these high pressures exhibits a pressure dependency similar to that of K_2CO_3 and Na_2CO_3 at low pressures, a supercritical fluid phase ascending from the lower parts of the upper mantle must experience a continuous and significant fractionation by either condensation of a liquid or crystallization of a series of carbonate minerals and produce Mg-rich and Ca-rich phase assemblages at different pressures. This suggests that the variability and compositional range of individual minerals as well as of whole-rock assemblages observed in carbonatite complexes, and perhaps in kimberlites as well, may be the result of fractional condensation and crystallization of a rapidly ascending supercritical fluid.

Acknowledgments

I thank S. Guggenheim and M.F.J. Flower for their constructive comments on the initial manuscript and D. B. Joyce and S. M. Sterner for helpful and critical reviews. Support by the Petroleum Research Fund of the American Chemical Society (grant 20016-AC2) and the National Science Foundation (grant EAR-8816898) is gratefully acknowledged.

References cited

Bailey, D.K. (1984) Kimberlite: "The mantle sample" formed by ultrametasomatism. In J. Kornprobst, Ed., Kimberlites, vol. I: Kimberlites and related rocks. Proceedings of the Third International Kimberlite Conference, p. 323–333, Elsevier, Amsterdam.

Boettcher, A.L., O'Neill, J.R., Windom, K.E., Steward, D.C., and Howard, K.G. (1979) Metasomatism of the upper mantle and the genesis of kimberlites and alkali basalts. In F.R. Boyd and H.O.A. Meyer, Eds., The mantle sample: Inclusions in kimberlites and other volcanics. Pro-

ceedings of the Second International Kimberlite Conference, vol. 2, p. 173–182, American Geophysical Union, Washington, D.C.

Boettcher, A.L., and Wyllie, P.J. (1969) The system CaO-SiO_2-CO_2-H_2O —III. Second critical end-point on the melting curve. Geochimica et Cosmochimica Acta, 33, 611–632.

Brown, M.E. (1988) Introduction to thermal analysis, 211 p. Chapman and Hall, New York.

Dawson, J.B. (1962) Sodium lavas from Oldoinyo Lengai, Tanganyika. Nature, 195, 1075–1076.

Dubois, C.G.B., Furst, J., Guest, N.J., and Jennings, J. (1963) Fresh natro carbonatite lava from Oldoinyo Lengai. Nature, 197, 445–446.

Eggler, D.H. (1987) Solubility of major and trace elements in mantle metasomatic fluids: Experimental constraints. In M.A. Menzies and C.J. Hawkesworth, Eds., Mantle metasomatism, p. 21–41. Academic Press, New York.

Eggler, D.H., and Rosenhauer, M. (1978) Carbon dioxide in silicate melts: II. Solubilities of CO_2 and H_2O in $CaMgSi_2O_6$ (Diopside) liquids and vapors at pressures to 40 kb. American Journal of Science, 278, 64–94.

Eggler, D.H., and Wendlandt, R.F. (1979) Experimental studies on the relationship between kimberlite magmas and partial melting of peridotites. In F.R. Boyd and H.O.A. Meyer, Eds., Kimberlites, diatremes, and diamonds: Their geology, petrology, and geochemistry. Proceedings of the Second International Kimberlite Conference, vol. 1, p. 330–338, American Geophysical Union, Washington, D.C.

Ellis, D., and Wyllie, P.J. (1979) Carbonation, hydration, and melting relations in the system MgO-H_2O-CO_2 at pressures up to 100 kbar. American Mineralogist, 64, 32–40.

Flynn, R.T., and Burnham, C. Wayne (1978) An experimental determination of rare earth partition coefficients between a chloride containing vapor phase and silicate melts. Geochimica et Cosmochimica Acta, 42, 685–701.

Freestone, I.C., and Hamilton, D.L. (1980) The role of liquid immiscibility in the genesis of carbonatites—An experimental study. Contributions to Mineralogy and Petrology, 73, 105–117.

Holloway, J.R. (1971) Internally heated pressure vessels. In G.C. Ulmer, Ed., Research for high pressure and temperature, p. 217–258. Springer-Verlag, New York.

Kjarsgaard, B.A., and Hamilton, D.L. (1988) Liquid immiscibility and the origin of alkali-poor carbonatites. Mineralogical Magazine, 52, 43–55.

Koster van Groos, A.F. (1975) The effect of high CO_2 pressure on alkalic rocks and its bearing on the formation of alkalic ultrabasic rocks and the associated carbonatites. American Journal of Science, 275, 163–185.

——— (1979) Differential thermal analysis of the system NaF-Na_2CO_3 to 10 kbar. Journal of Physics and Chemistry, 83, 2976–2978.

Koster van Groos, A.F., and ter Heege, J.P. (1973) The high-low quartz transition to 1 kilobar pressure. Journal of Geology, 81, 717–724.

Koster van Groos, A.F., and Wyllie, P.J. (1963) Experimental data bearing on the role of liquid immiscibility in the genesis of carbonatites. Nature, 199, 801.

——— (1968) Liquid immiscibility in the join $NaAlSi_3O_8$-Na_2CO_3-H_2O and its bearing on the genesis of carbonatites. American Journal of Science, 266, 932–967.

——— (1973) Liquid immiscibility in the join $NaAlSi_3O_8$-$CaAl_2Si_2O_8$-Na_2CO_3-H_2O. American Journal of Science, 273, 465–487.

Le Bas, M.J. (1981) Carbonatite magmas. Mineralogical Magazine, 44, 133–140.

Menzies, M.A., and Wass, S.Y. (1983) CO_2 and LREE-rich mantle below eastern Australia: A REE and isotopic study of alkaline magmas and apatite-rich mantle xenoliths from the Southern Highlands Province, Australia. Earth and Planetary Science Letters, 65, 287–302.

Morey, G.W., and Chen, W.T. (1956) Pressure and temperature curves in some systems containing water and a salt. Journal of the American Chemical Society, 78, 4249–4252.

Novgorodov, G.P. (1975) Quartz solubility in H_2O-CO_2 mixtures at 700 °C and pressures of 3 and 5 kbar. Geokhimica, 10, 1484–1489.

Rankin, A.H. (1977) Fluid inclusion evidence for the formation conditions of apatite from the Tore carbonatite complex of eastern Uganda. Mineralogical Magazine, 41, 155–164.

Ricci, J.E. (1951) The phase rule and heterogeneous equilibrium, 505 p. Van Nostrand Co., New York.

Roden, M.F., and Murthy, V.R. (1985) Mantle metasomatism. Annual Review of Earth and Planetary Science, 13, 269–296.

Schneider, M.E., and Eggler, D.H. (1984) Compositions in equilibrium with peridotite: Implications for alkaline magmatism-metasomatism. In J. Kornprobst, Ed., Kimberlites, vol. I: Kimberlites and related rocks. Proceedings of the Third International Kimberlite Conference, p. 383–403, Elsevier, Amsterdam.

——— (1986) Fluid in equilibrium with peridotite minerals: Implications for mantle metasomatism. Geochimica et Cosmochimica Acta, 50, 711–724.

Scott, B.H. (1979) Petrogenesis of kimberlites and associated lamprophyres from Central West Greenland. In F.R. Boyd and H.O.A. Meyer, Eds., Kimberlites, diatremes, and diamonds: Their geology, petrology, and geochemistry. Proceedings of the Second International Kimberlite Conference, vol. 1, p. 190–205, American Geophysical Union, Washington, D.C.

Shettel, D.L. (1973) Solubilities of quartz in H_2O-CO_2 fluids at 5 kb and 500–900 °C. EOS, 54, 480.

Smykatz-Kloss, W. (1974) Differential thermal analysis, 185 p. Springer Verlag, New York.

Spera, F.J. (1987) Dynamics of translithospheric migration of metasomatic fluid and alkaline magma. In M.A. Menzies and C.J. Hawkesworth, Eds., Mantle metasomatism, p. 1–20. Academic Press, New York.

Tranquard, A. (1965) Contribution a l'étude du système ternaire eau-soude-carbonate de sodium, 42 p. Thèse Doctorat Science Physique, Gauthier-Villars, Paris.

Von Eckermann, H. (1948) The alkaline district of Alno Island. Sveriges Geologiska Undersokning, No. 36, 176 p.

Waldeck, W.F., Lynn, G., and Hill, A.E. (1932) Aqueous solubility of salts at high temperatures. I. Solubility of sodium carbonate from 50 to 348 °. Journal of the American Chemical Society, 54, 928–936.

Wallace, M.E., and Green, D.H. (1988) An experimental determination of primary carbonatite magma composition. Nature, 335, 343–346.

Walther, J.V., and Orville, P.M. (1983) The extraction quench technique for determination of the thermodynamic properties of solute complexes: Application to quartz solubility in fluid mixtures. American Mineralogist, 68, 731–741.

Wass, S.Y. (1979) Fractional crystallization in the mantle of late-stage kimberlitic liquids—Evidence in xenoliths from the Kiama area, N.S.W., Australia. In F.R. Boyd and H.O.A. Meyer, Eds., Kimberlites, diatremes, and diamonds: Their geology, petrology, and geochemistry. Proceedings of the Second International Kimberlite Conference, vol. 1, p. 336–373, American Geophysical Union, Washington, D.C.

Wendlandt, R.F. (1984) An experimental and theoretical analysis of partial melting in the system $KAlSiO_4$-CaO-MgO-SiO_2-CO_2 and application to the genesis of potassic magmas, carbonatites and kimberlites. In J. Kornprobst, Ed., Kimberlites, vol. I: Kimberlites and related rocks. Proceedings of the Third International Kimberlite Conference, p. 359–369, Elsevier, Amsterdam.

Wendlandt, R.F., and Harrison, W.J. (1979) Rare earth partitioning between immiscible carbonate and silicate liquids and CO_2 vapor. Results and implication for the formation of light earth enriched rocks. Contributions to Mineralogy and Petrology, 69, 409–419.

Wendlandt, W.W. (1974) Thermal methods of analysis (2nd Edition), 505 p. Wiley & Sons, New York.

Wyllie, P.J. (1980) Origin of kimberlites. Journal of Geophysical Research, 85, 6902–6910.

——— (1987) Transfer of subcratonic carbon into kimberlites and rare earth carbonatites. In B.O. Mysen, Ed., Magmatic processes, 500 p. The Geochemical Society, Pennsylvania State University, University Park, PA.

Wyllie, P.J., and Boettcher, A.L. (1969) Liquidus phase relationships in the system CaO-CO_2-H_2O to 40 kilobars pressure with petrological applications. American Journal of Science, 267-A, 489–508.

Yoder, H.S., Jr. (1950) High-low quartz inversion up to 10,000 bars. Transactions of the American Geophysical Union, 31, 827–835.

MANUSCRIPT RECEIVED APRIL 24, 1989
MANUSCRIPT ACCEPTED FEBRUARY 7, 1990